



**Czech
Technical
University
in Prague**

F3

**Faculty of Electrical Engineering
Department of Cybernetics**

Bachelor's Thesis

Distributed control of an array of light sources

Author: **Křištof Pučejdl**
Supervisor: **Ing. Zdeněk Hurák, Ph.D.**
Thesis submission: **May 2016**

BACHELOR PROJECT ASSIGNMENT

Student: Křištof P u č e j d l
Study programme: Cybernetics and Robotics
Specialisation: Robotics
Title of Bachelor Project: Distributed Control of an Array of Light Sources

Guidelines:

Design and build a prototype of an experimental platform consisting of a regular array (1D or 2D, at least 4x1 or perhaps even 4x4) of independently programmable modules that contain light sources (LEDs) as well as the electronics needed for force interaction (magnetic, mechanical, electrostatic, ...) with the neighbors. The platform is intended to be used for visualization of some wave phenomena in multiagent systems. Perform some basic analysis both using the mathematical model and the data obtained from the experimental setup, and propose, implement and test some control strategies.

Bibliography/Sources:

- [1] J. Zemánek, Z. Hurák: Experimental modular platform for distributed planar manipulation by shaping magnetic field. Sent for publication. 2015.
- [2] Z. Hurák, J. Zemánek: Feedback linearization approach to distributed feedback manipulation, In proc. American Control Conference (ACC), Montréal, Canada, pp. 991-996, June 2012. DOI: 10.1109/ACC.2012.6315262.
- [3] D. Martinec, I. Herman, Z. Hurák, and M. Šebek: "Wave-absorbing vehicular platoon controller", European Journal of Control, vol. 20, no. 5, pp. 237-248, Sep. 2014.

Bachelor Project Supervisor: Ing. Zdeněk Hurák, Ph.D.

Valid until: the end of the summer semester of academic year 2016/2017

L.S.

prof. Dr. Ing. Jan Kybic
Head of Department

prof. Ing. Pavel Ripka, CSc.
Dean

Prague, December 16, 2015

Declaration

I declare that the presented work was developed independently and that I have listed all sources of information used within it in accordance with the methodical instructions for observing the ethical principles in the preparation of university theses.

Prague, date _____

signature

Acknowledgements

First, I would like to thank my supervisor Ing. Zdeněk Hurák, Ph.D. for his advices and support. Next I owe my big gratitude to mr. Ladislav Čmelík who built the main frame for the platform, to Doc. Ing. Petr Kašpar, CSc. for providing me with an access to the coil winding machine and all the needed guidance regarding its operation, and to Ing. Jiří Zemánek for his help with the fabrication of custom parts. Finally, I would like to thank my family for their continuous love and support.

Abstract

This bachelor's thesis is concerned with designing, building and testing of a prototype of an experimental electromechanical platform that consist of a set of individually programmable modules which can interact via force and conceive motion. The aim for such platform is to visualize some wave phenomena in multi-agent systems and to offer a scope for designing and testing of control algorithms. Because of the reasons explained later in the thesis, the platform has not been finished into its final form specified in the assignment, and the main content of this thesis documents the construction of a 'proof-of-concept' prototype. Based on the experiences and observations acquired during this prototyping stage, the final form and features of the full platform are proposed along with several suggestions for hardware improvements. Lastly the base of the mathematical model is derived for the platform in the proposed form.

Keywords: experimental platform, 3D print, prototyping, electromagnetism, coil, multi-agent systems, Lagrange's equations

Abstrakt

Obsahem této bakalářské práce je návrh, stavba a testování prototypu experimentální elektromechanické platformy, jež sestává ze skupiny samostatně programovatelných jednotek, které na sebe mohou vzájemně působit silou a vykazovat tak pohyb. Platforma by měla sloužit k vizualizaci vlnových jevů v multiagentních systémech a rovněž k návrhu a testování řídicích algoritmů. Vzhledem k důvodům blíže popsáným v samotné práci nebyla platforma dokončena do své finální podoby specifikované v zadání práce, a hlavní náplní je stavba prototypu k ověření celkového konceptu platformy. Na základě zkušeností a zjištění získaných při jeho návrhu a konstrukci jsou pak navrženy finální podoba a funkce kompletní platformy včetně několika doporučení na možná vylepšení. V závěru práce je odvozen obecný matematický model popisující platformu v její plně navržené podobě.

Klíčová slova: experimentální platforma, 3D tisk, prototypování, elektromagnetismus, cívka, multiagentní systémy, Lagrangeovy rovnice

Contents

1 Introduction	1
1.1 Motivation	1
1.2 Achieved Goals	1
1.3 Thesis Outline	2
Part I	
Prototype Platform	
2 Initial Concept	5
3 Physical Domain of Module Interaction	7
3.1 Mechanical interaction	7
3.2 Magnetic interaction	8
4 Determining the Scale	9
5 Sensors and Measurements	11
5.1 Requirements for measured variables	11
5.2 Measuring the Distance between Adjacent Modules	12
5.2.1 Distance Sensors Challenges	13
5.3 Absolute Position Measurement	14
5.3.1 Inertial Measurement	14
5.3.2 Vision-based Position Measurement	14
6 Designing and Building	15
6.1 3D Printing	15
6.2 Coil Design and Fabrication	16
6.3 Spherical Hinges and the Frame	19
6.4 Pendulum Module	21
6.4.1 The electronics	21
6.4.2 3D Printed Parts	24
6.4.3 Module Assembly	25
Part II	
Mathematical Model	
7 General Mathematical Model	29
7.1 Simplifying Assumptions	29
7.2 Lagrange's Equations	30
7.2.1 Generalized Coordinates	30
7.2.2 Energies in the System	33
7.2.3 Differential Equations	34
7.3 State Space Model	36
8 System Parameters and Identification	39
8.1 Pendulum Characteristics	39
8.2 Force Interaction	40
8.2.1 Force Measurement	41
9 Conclusion	43
9.1 Future Work	44

Bibliography	I
Appendices	
A Contents of the enclosed CD	V



Chapter 1

Introduction

This bachelor's thesis deals with design and build of an electromechanical platform consisting of a set of individually programmable modules which can mutually interact by force and perform a motion. The setup should allow using a distributed control algorithms, utilizing microprocessor units of each module, and all modules should be equipped with light sources for a better visualization of the motion. Ultimately, the platform is expected to be used for developing, observing of some wave phenomena in given multi-agent system, and for designing control algorithms for such systems.



1.1 Motivation

Experimental platforms like this one are often built to imitate some other physical system that is difficult to work with, either from the reasons of scale, required energy or limitations in resources etc. In such case, it is usually given what properties should the platform have and what performance is expected from it.

In my case on contrary, the goal is less specific and offers whole variety of approaches and paths to choose. I also expected that the final shape and function of the device along with some performance tests will inspire and determine the further experiments, while a lot of the actual research will contain discovering of what all can be achieved with given platform and what challenges regarding the control efforts are there.



1.2 Achieved Goals

The final result achieved in this project may seem to lag behind of what the assignment and especially the title suggested. Rather than explaining this in the conclusion only, let me address this issue straight ahead and—with no intention to tergiversate—provide some clarification.

When beginning with this project, all I had was an abstract idea. Everything regarding physical form of the device and its practical realization was to be determined. A lot of the initial ideas proved to be non-functional and the more we were stepping into the problematic, the more it was clear that a lot of testing and prototyping would be necessary. Therefore, this whole project turned into rather 'proof of concept' type of work. The main focus was to build a rough prototype to try the ideas, principles and methods in order to prove or disprove their feasibility for the potential final device.

1.3 Thesis Outline

The thesis is divided into two parts. The first and main Part I describes the whole process of the fabrication of the experimental platform. It begins with the closer inspection of the the initial concept along with the list of its desired properties and functions, which is followed by throughout description of the design process with all the decisions that has been made during the prototyping and also all the pitfalls and challenges that had to be overcome. Lastly, the final assembly is described in the Part I.

Part II contains a sketch of the mathematical model that generally describe the platform in its desired final form and introduces several methods which are used for system identification. Rather than providing some completed results within the prototype platform, this part is directed ahead towards the full platform, providing an insight to the problem and some guidelines to the future work.



Part I

Prototype Platform

Chapter 2

Initial Concept

The initial idea for the platform is mostly described in the official assignment to this thesis and in the Chapter 1 on page 1. This section only extends this description with some additional thoughts and ideas I had to the start and provides an insight into the overall problematics. Since the very beginning, there has been the following general idea:

- The platform should consist of a regular, preferably 2D array of independent modules.
- Each module should be able to measure the distances from its neighbours.
- There should be a way for each neighbours to physically interact in form of attraction and repulsion. However, there should not be any form of rigid linkage between the modules—possible connection should always be flexible.
- The range of motion for each module, while heavily depending on the overall scale, should be at least several centimeters.¹

In the assignment, there also is a note about the presence of LED lights on the modules. This feature, however, was only meant for the purposes of better visualization, thus being of very low priority regarding the actual experimental function. Since the inclusion of such feature only makes sense with the finalized platform, it has not been dealt with in this work.

In the early stages of the project I was considering several possible principles which the platform could utilize—omni-directional carts or small floating objects in the water tank to name a few. Ultimately, the prevailing idea was to have the modules hanging on a piece of string or wire, thus forming spherical pendulums. The reason for such decision was that such implementation introduces an oscillatory behavior with the fixed equilibrium to the system and as such it offers both more opportunities and additional challenges to the experiments. At the time I also thought that the realization of the pendulum based platform should be reasonably easy, at least compared to the other options. Although it is impossible to objectively measure the actual difficulty, it must be acknowledged that it turned out to be far more challenging than I originally anticipated.

¹That is for the motion to be obvious to the human eye.

Chapter 3

Physical Domain of Module Interaction

Once the general pendulum-based principle of the platform had been selected, the very first issue I had to address was the choice of physical domain for the force interaction between the modules. Two possible ways were considered, one being from mechanical domain, the other from the domain of electromagnetism.

3.1 Mechanical interaction

The idea of mechanical principle involved servo-driven spring linkage between the neighbours. Figure 3.1 shows the general idea for the linkage between modules M_1 and M_2 .

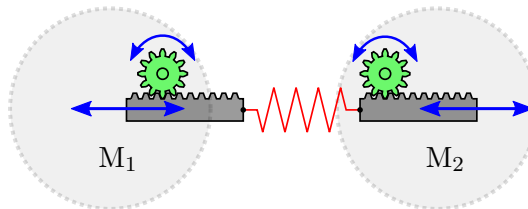


Figure 3.1: Possible principle of mechanical interaction.

The spring is rigidly connected to the ratchets which are operated by small servo motors. The main advantage of such implementation is the constant force within the full range of motion of these ratchets. It would, however, require quite sophisticated mechanics for it to work properly, along with some sort of special spring assembly that prevents it from bending (something like soft shock absorber could be an option) and also the size and the weight of the modules would increase rapidly with the servo motors.

The biggest problem that eventually led to rejection of this solution was the need for unrestricted motion in both axis and the possibility of having zero force interaction between two modules. Both of these properties would be very hard to reach with given mechanical setup. Even if the spring linkage allowed some side to side movement of the modules (in the axis perpendicular to the linkage direction), there would always be big damping. For the zero force interaction, there is no way to effectively reach it without physically disengaging the spring linkages.

3.2 Magnetic interaction

The alternative way was to harness a magnetic field. The original idea was to have a single vertically oriented electromagnet in each module. When energized, these would act as cylindrical bar magnets and in theory, such setup should work as Figure 3.2a suggests.

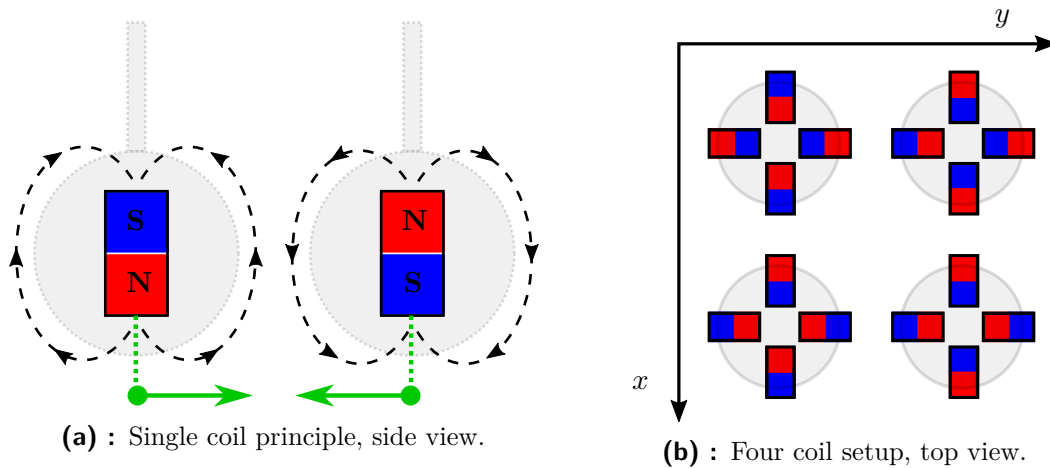


Figure 3.2: Possible principles of magnetic interaction.

If both of the magnets are oriented the same way, the modules repulse each other, otherwise, they attract each other. Unfortunately, the experiments proved that in this orientation the effective reach of the magnetic field is extremely short and especially the repulsion effect was close to none with any distance greater than zero. In this case, using very long coils could possibly help, yet due to the other disadvantage which is the inability to control the direction of the magnetic force within the horizontal plane,¹ I eventually decided to scratch this idea.

The alternative and currently the final implementation is that each module includes four² coils, one facing each of its neighbours (see the Figure 3.2b). That allows for controlling the individual interactions and presumably also longer effective reach of the magnetic force.

Ultimately, using magnetic interaction not only requires far less mechanical elements but also allows for zero force interaction and unrestricted perpendicular movement when both opposing electromagnets are disabled. The only possible disadvantage I initially anticipated was the low reach of effective magnetic field. Nevertheless, this implementation was a certain choice at the time. Only the further work proved that there are other disadvantages and that this solution is not as ideal as it seemed to be.

¹That means inability to create certain interaction between two modules without affecting the other neighbours.

²I assume the square matrix layout of the modules. There could be other options, e.g. hexagonal or triangular. These would require three or six coils per module respectively.

Chapter 4

Determining the Scale

Second important step was to select the scale and the dimensions for whole platform and its components. The size of the platform is mostly determined by the size of one pendulum module. The desire was to make the modules as small as possible so the whole platform is of a manageable ‘desktop’ size. Having nothing but this general requirement, it was clear that some arbitrary choices followed by testing experiments were inevitable.

As a determining element for the module’ size I first selected the coils acting as electromagnets. For the initial tests, small coils which used to operate small latching relays seemed to be an eligible choice.

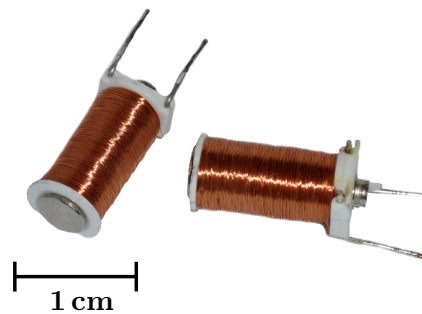


Figure 4.1: Picture of the small coils from disassembled latching relays.

Unfortunately, the experiments proved that the magnetic field provided by these coils has by far insufficient reach and even on small distances $d < 1$ cm it would be barely able to move the module no matter how light weight would it be.

Having learned this, I decided to base the size of the coils on the estimation of the module size and weight. Since I did not have any specific plans on what electronic components to use, I could only make a rough estimation that the module should fit inside the sphere of a diameter of 10 cm and the weight of the assembly without the coils should be about 100 g. Based on these estimations I decided the coils to approximately fit into the cube with the side length of 3 cm.

Another important property that has to be determined was the length of the pendulum cord. I needed the modules to be able to move at least several centimeters in each direction without the pendulum angles going to big so that I can neglect the vertical ‘raise’ and assume that the modules move in the horizontal plane. Therefore, I decided for the length l of the pendulums cord to be 60 cm. With horizontal

displacement $\Delta = 5$ cm that gives less than the angle deflection from the vertical axis $\theta < 5^\circ$ and the maximal vertical raise of approximately 0.2 cm.

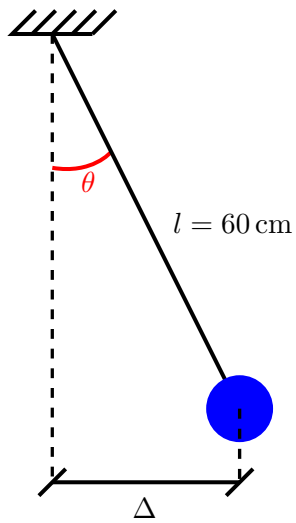


Figure 4.2: Supporting image for the size description.

The final spacing between pendulums heavily depends on the module dimensions and coil performance so at this stage I could only estimate it to be between 10 cm and 15 cm.

Chapter 5

Sensors and Measurements

5.1 Requirements for measured variables

The aim for this platform is to have a multi-agent system with a distributed control so that each module regulates the current on its coils independently. The requirement of modularity also restricts me from using any kind of external measurement method. Everything shall be done within the modules.

Let's now inspect the situation where two adjacent modules interact via their opposing coils. Given by the nature of such system, there are two key phenomena that need to be acknowledged. First, the force interaction between the neighbours is always mutual and opposite. Second, the strength and sense (attraction/repulsion) of such interaction depends on all following factors:

- Currents i_A and i_B through both opposing coils of the modules M_A and M_B .
- Parallel distance d between the modules.
- Perpendicular offset δ of the modules.¹

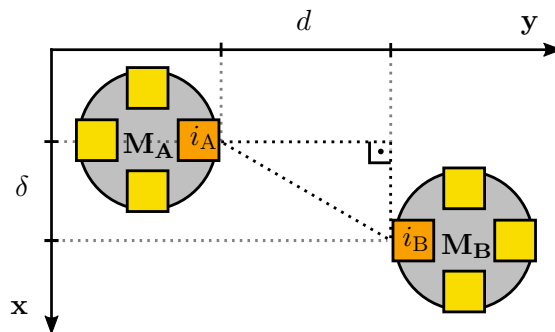


Figure 5.1: Two interacting modules viewed from above. Orange squares represent the coils, darker coils are active in given interaction.

This means that in order to compute the correct action input, module needs to know its own position and velocity² and also the positions of its neighbour and the electric currents through the respective coils involved in the interaction.

¹The magnetic force is strongest for $\delta = 0$. With any of the coils offset to the side, the effect of the magnetic field decreases rapidly.

²Velocity is required because the dynamics of the mechanical part of the system is described by

5.2 Measuring the Distance between Adjacent Modules

For measuring the distance, using direct measurement via distance sensors is a logical option to consider. Because of the need of knowing the neighbour's electric current it was certain that some kind of communication between the modules had to be included. Since I already knew that, I could use data sharing for the distance measurements as well in order to reduce the number of required sensors. As seen on the Figure 5.2, instead of having four sensors on each module to monitor each of its neighbours, only two sensors per module would be enough if I used data sharing. Yellow sensors are redundant in the illustrated layout and could be omitted, although it would be at the expense of the module universality and the ease of platform extension.

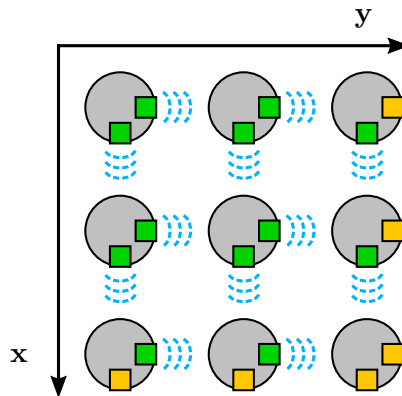


Figure 5.2: Possible implementation of distance sensor, seen from above. The circles represent the modules, small squares represent the distance sensors.

For my application, I specified several requirements for such sensor:

- The range starting from nearly a zero and extending up to at least 5 cm.,
- The resolution within this range at least ± 1 mm,
- The sampling rate at least 50 Hz,³
- Reasonably small size of the pendulum module (10 cm diameter),
- Ideally, no requirement for any kind of distinct reflective surface on the detected object.⁴

Last but not least criterion was the price. There are compact and high precision industrial laser triangulation sensors available that easily meet and exceeds my requirements. Such sensors, however, currently cost at least about \$300.

More affordable sensors usually use either ultrasonic or infrared reflection principle. The ultrasonic sensors with acceptable price usually feature lower resolution for very

the system of 2nd order differential equations. However, the velocity is almost exclusively obtained by computing the derivation of the position and therefore does not add any new requirement for measurement.

³Slower sampling rate may be insufficient for control algorithms.

⁴Relying on reflexive surface is a less flexible method and may introduce complications with any further design change on the modules.

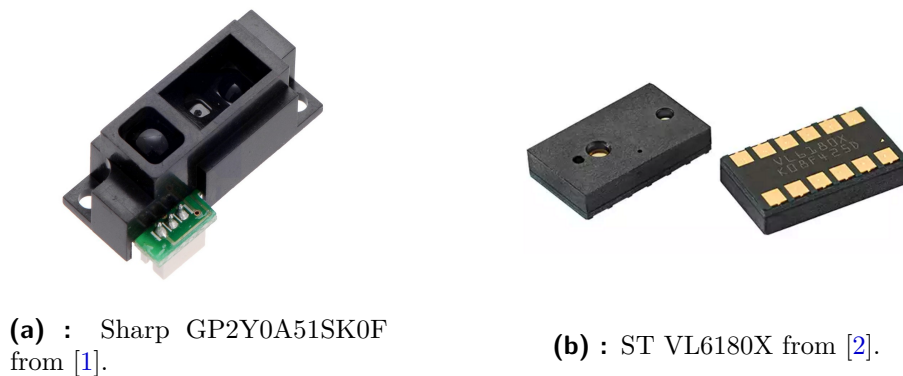


Figure 5.3: Distance sensors.

short range and are usually bigger than what I aimed for. From the infrared reflection sensors, the GP2Y0A51SK0F made by Sharp seem to combine most of the desired characteristics. Unfortunately, according to the datasheet [1] its effective range starts at 2 cm which would require the sensor to be built deeper inside of the modules.

Another option would be the Proximity and Ambient Light Sensing (ALS) module VL6180X from the manufacturer ST. According to the technical specifications [2], this sensor has an effective range starting at zero and utilizes the Time-of-Flight technology i.e. it precisely measures the time it takes to the light to reach the object and get back to the sensor. That provides more accurate measurement than the standard reflection technology, which measures the amount of reflected light and as such is highly influenced by the surface and color of the detected object. There were two reasons for me not to try this sensor in the end. First, it is an SMD (Surface Mount Device) component which would require a custom PCB (Printed Circuit Board) for the implementation. Second, it was relatively new release at time, not yet offered by suppliers.

5.2.1 Distance Sensors Challenges

Although the use of distance sensors first appeared as very practical, I soon found some major issues that spoil the proper functionality of such sensors, regardless the type. All of these sensors have very narrow radius of detection, which would cause troubles in the situations like the one illustrated on the Figure 5.4 on the next page.

The detection only works properly when the two adjacent modules are in line with the sensor axis (green sensors). If the observed module is deflected sideways (red sensors), the measurement is very inaccurate or completely lost for bigger deflection. This situation, unfortunately, is expected to be very common within the platform.

Another disadvantage of utilizing such sensor type is the fact that even if accurate measurements were granted at all times, I can only derive the relative positions from such data, because all the sensors are mounted on movable modules. However, given by the pendulum-based nature, the dynamics depends on the absolute deviation of the modules. Ultimately, this leads to the requirement for measuring the absolute positions of the modules.

Because of the reasons stated above, I eventually decided not to use distance

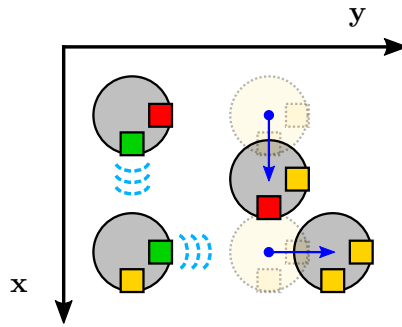


Figure 5.4: Situation with reduced functionality of a distance sensor, seen from above. The circles represent the modules, small squares represent the distance sensors.

sensors at the time. However, these are still being considered as complementary sensors for improving the accuracy and reliability of the measurements.

■ 5.3 Absolute Position Measurement

■ 5.3.1 Inertial Measurement

One option for measuring the absolute position of the modules is using an inertial measurement unit (IMU). Such device usually consists of three-axis accelerometer complemented with gyroscopic sensor and provides information about its spatial orientation. The advantages of this method are mainly the availability, price and small size of such sensor units. Possible disadvantages with respect to my application are low resolution and the presence of a cumulative error⁵ within the on board sensors.

Despite the disadvantages, I decided to use this method instead of another mentioned below. The specific device and its implementation is described in detail in the Section 6.4.1 on page 22.

■ 5.3.2 Vision-based Position Measurement

The alternative I was considering for absolute position detection was using a small camera on the bottom of each module along with grid-marked ground cloth underneath the modules. Combining an appropriate camera with a distinct grid or mesh pattern on the base and corresponding image processing software could very well result in the very precise and reliable measurement. Furthermore, using a reference marks for each module zero position could prevent any cumulative error.

As long as utilizing such method would require a lot of experimenting and additional work, I decided not to attempt for it within this thesis. In case of an unsatisfactory accuracy of the IMU however, testing this method is recommended for the further development on this project, either as an extended calibration option or even as main measurement method.

⁵Small errors introduced in each measurement cycle add up over time and there is no way for the sensor to eliminate these. For sensors with gyroscopic module, however, this error is usually negligible unless the sensor runs for very long time period without being calibrated.

Chapter 6

Designing and Building

In this section, the process of designing and building of the prototype platform is described. It summarizes the important steps and although it does not cover each step extensively, several parts are described in detail to point out some important attributes of the build. Sometimes there were more iterations of certain element design than mentioned and the unsuccessful attempts are mostly omitted, unless there was some valuable experience as a result.

6.1 3D Printing

3D printing technology and printed parts were used extensively throughout the build of this platform. For better clarity, let me summarize general regarding information in this section. The individual designs and associated issues are described in respective following chapters.

I designed all the 3D printed parts in the Autodesk 123D Design¹ software, which is a free software available to download. As such it lacks a lot of the features known from professional CAD² programs but is very useful for fast and easy design prototyping.

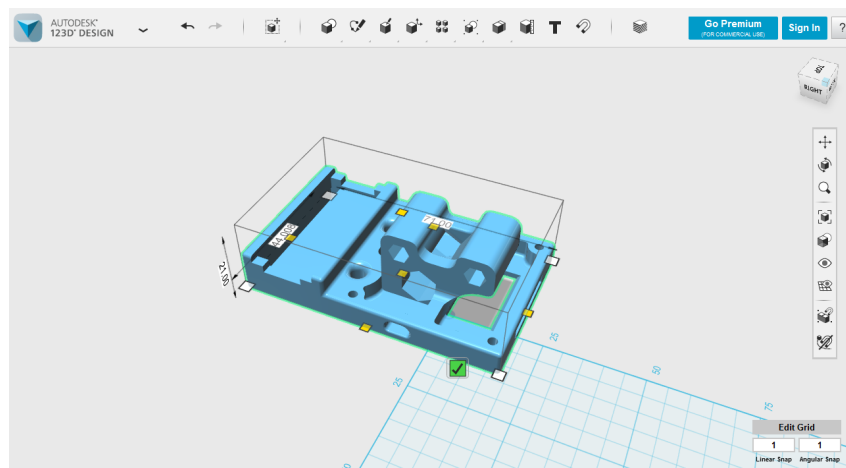


Figure 6.1: Screenshot of the 123D Design CAD environment.

¹<http://www.123dapp.com/>

²Computer Aided Design

All 3D files for the parts used in this build are attached on the enclosed CD in both editable and printable formats (see the Appendix A).

I further processed all 3D files in Cura³, which is a free software, commonly referred to as a ‘slicer’. Such software plans the layered tool path for the printing head with respect to the design, given 3D printer and optional user settings such as printing speed, quality etc.

For the actual printing I used the Ultimaker 2⁺ 3D printer⁴ available at the Department of Control Engineering in the Faculty of Electrical Engineering at Czech Technical University in Prague. As a printing material, PLA plastic was used for all the components. On top of otherwise very good properties, such as hardness and durability, this common 3D printing filament suffer from one negative attribute which is its low glass transition temperature about 65 °C. I did not consider this property in advance and it caused some complications regarding the coil design. This issue is further referred to in the next chapter.

For most of the printing, I used recommended print settings⁵ for given filament and used 0.4 mm nozzle. The infill density ranged between 20% and 100% according to the shape of the individual parts.

6.2 Coil Design and Fabrication

I did not have any coils available that would fit my needs so it was necessary to design and fabricate these. The coil formers⁶ were designed and printed on 3D printer. The first functional former design is shown on the Figure 6.2. It accepts M6 iron bolt as a ferromagnetic core and the mounting holes fit a M3 machine screw.

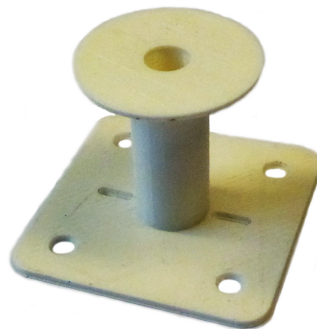


Figure 6.2: Picture of the 3D printed coil former.

I manually wound all the coils used in this project on an old winding machine which is located in the basement of the Department of Circuit Theory within the CTU in Prague. The access to this machine was kindly granted by doc. Ing. Petr Kašpar, CSc., who also provided me with all the training and counseling.

³<https://ultimaker.com/en/products/cura-software>

⁴<https://ultimaker.com/en/products/ultimaker-2-plus>

⁵E.g. printing speed, layer height, shell thickness etc.

⁶The plastic ‘spool’ which holds the winding.

Now let me analyze the choice of the wire for the coil windings. For the value of the magnetic flux density B of the coil in certain fixed point near the coil we can write that

$$B \propto N I_w, \quad (6.1)$$

where N is the number of turns in the coil winding and I_w is the electric current that flows through the winding. Therefore, in order to reach the maximal B , I needed to maximize this product $N I_w$, commonly referred to as ‘ampere-turns’. The approximate number of turns in given hollow cylindrical body of the coil is inversely proportional to the cross-section area S of the wire but so is the electrical resistance R of the wire. Furthermore, R is proportional to the length of the wire, which means that using thinner and longer wire to gain more turns results in significantly bigger resistance and that raises the requirement for input voltage level accordingly. This fact may suggest that such method of getting stronger magnetic field is not adequate and that I should rather focus on increasing the current through a thicker wire winding. However, another phenomena steps in at this point – a Joule heating H . According to the Joule’s first law,

$$H \propto I_w^2 R t \quad (6.2)$$

which effectively limits the available current, while using high current could easily overheat and even burn the device.

This being said it is obvious that there was no secure way to determine the wire thickness without experimenting. Therefore, I wound three coils using 0.27 mm, 0.35 mm and 0.5 mm copper wire⁷ which have approximately 1000, 600 and 400 turns respectively. With these coils hanging on a string I measured how close did I have to place small iron cylinder in order to have the coil attracted to it. The maximum voltage was set to 24 V for the purposes of potential battery powered modules, and within this voltage range, only the coil with 1000 turns provided the field strong enough to attract the cylinder at the distance of approximately 4 cm.

It was at this point where I decided not to aim onto big 2D array platform right then but to optimize the design and performance first with just two pendulums. Not only was the performance of the coils below my expectations—the magnetic field drop off effect was more significant than I initially estimated—but it was also clear that there would be more similar issues to experiment and deal with throughout further design. Therefore, any investments in manufactured parts (four coils per each module) would be risky before the whole concept is proved working.

Despite the lacking performance, I proceeded with the most effective 1000 turn coils and made four of those to accommodate two modules in 1D array arrangement. However, during one of the experiments with the preliminary setup seen on Figure 6.3 on the following page, one of the coils which was under 1 A current load for several seconds started to bend down. That was a result of a PLA plastic former starting to soften because of the high temperature of the coil.

As it was impossible to maintain the temperature of the coil sufficiently far below 60 °C, I had to strengthen the coil former using a hand-made aluminium bracket

⁷The dimensions stand for the wire diameter. The thickness of the insulation coating is not included.

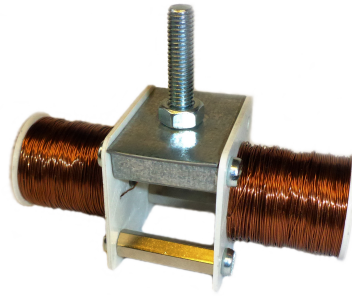
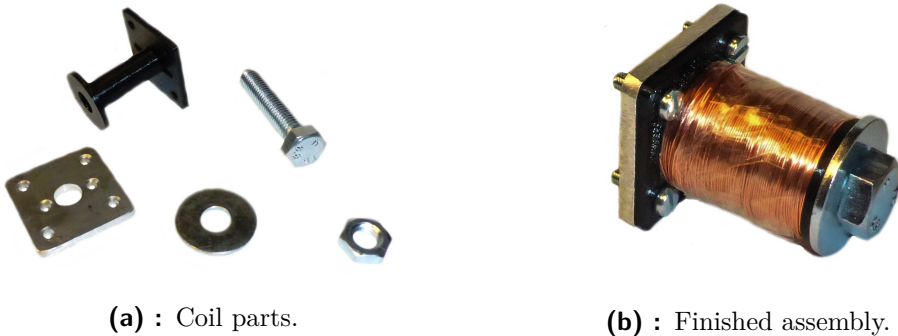


Figure 6.3: Picture of the preliminary module setup with two coils attached.

and a washer which were bolted onto the coil using longer core bolt and a hex nut. Despite adding some unwanted extra weight, this assembly proved to be very effective and the coils no longer suffered from the higher temperatures.

Unfortunately, the thermal and mechanical stress that have been put onto the coils during further manipulation and experiments caused two of them getting incorrigibly damaged. Since this happened at the point where the rest of the module assembly was nearing completion, I decided to completely remake these coils, using slightly bigger and strengthened former (see the Figure 6.4a), which allows for using 0.35 mm wire while keeping the 1000 turns. The final coil assembly is shown on the Figure 6.4b.



(a) : Coil parts.

(b) : Finished assembly.

Figure 6.4: Pictures of the final form of the coil.

This coil design in terms of shape and wire properties may not be ideal for given purpose because there is still very significant decrease of the force with the increasing distance. Regarding the question of extending the reach of effective magnetic field as much as possible, there are different approaches to try. One would be making the coil wide and flat so the magnetic field lines extend further before closing into loops. Another would be trying the very opposite, where the argumentation is that the further away the poles are, the less are these acting ‘against’ each other for low relative distances. Using several coils oriented in form of short Halbach array⁸ could also increase the magnetic force, yet that would be difficult to implement.

There was not enough time to test any of these improvements within this bachelor thesis but it is certainly recommended for the for the further work on this project.

⁸Special arrangement of magnets that augments the magnetic field on one side of the array while canceling the field to near zero on the other side. [3]

6.3 Spherical Hinges and the Frame

The frame for two-pendulum platform was made from standard 20×20 mm aluminium profile extrusions. It is 74 cm high and 34 cm wide. The picture of the bare frame is on the Figure 6.5.



Figure 6.5: The frame for the prototype platform

The original idea for the pendulum hanger was just a wire of some sort. The problem I did not realize till I actually tested the first small coils on the wire was the unwanted rotation of the modules. Especially during the repulsion, rather than actually pushing away each other, the coils just rotated. Since I needed to maintain the module orientation with respect to the horizontal axis, it was clear that any kind of string or wire was insufficient and that some rigid rod would be required. I decided to use hollow aluminium tube of 5 mm diameter. Such tube is very stiff against torsion and also allows to run power wires through it so the modules can be powered from the outside source with the wires conveniently hidden inside the pendulum rods.

The challenge was how to make the spherical hinge that would allow the rod to swing any direction but would prevent it from rotating around its axis. The first solution I came up with was using the short segment of rubber tubing as a connection between the rod and the bolt coming through the top crossbeam, see the Figure 6.6a on the following page.

At such short length, rubber tubing proved to be very stiff against torsion and allowed almost no rotation in the joint even when relatively big torque was applied. The solution seemed perfect but later during testing I found out that such joint is to resistive against bending, thus introduces great damping to the pendulum oscillations

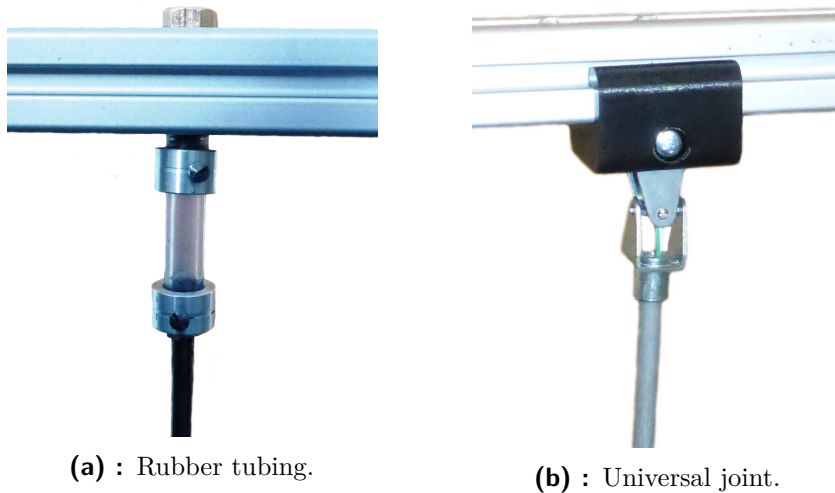


Figure 6.6: Pictures of two spherical hinge implementations.

and also too much counterforce for the coils to fight against when attempting to deflect the pendulum.

The other solution was to use universal joints. I used steel universal joints from the Merkur⁹ construction set while these fit my needs perfectly. Only small modifications had to be made on these parts.¹⁰ The final assembly is shown on the Figure 6.6b

The black bracket is 3D printed part which holds the universal joint. It was designed so it can slide along the top beam of aluminium extrusion with right amount of friction so it does not move unless it is strongly pushed either side. That allows for the distance between the pendulums to be easily adjusted without need for any structural modifications.

Although it is critical for the final platform that consist of 2D array of modules to implement these universal joints so the pendulums are allowed for spherical movement, for the purpose of testing on my simplified 1D prototype I needed to be able to restrict the movement within the single plane. For that purpose, I designed and printed two small parts which can slide into the opposing channels of the vertical aluminium extrusions within the frame and a two pieces of string or wire can be routed between those parts, creating a narrow channel in which the pendulum rod can move (see the Figure 6.7 on the facing page). That effectively prevents any side to side movement, which was especially useful during the initial attraction and repulsion tests and will also help with the system identification within the full 2D array platform (see the Section 8.1 on page 39).

⁹<http://www.merkurtoys.cz/en/>

¹⁰E.g. cutting the threads into one hub of the joint so the pendulum rod can be screwed in or drilling the hole through the center for the wires to go through.

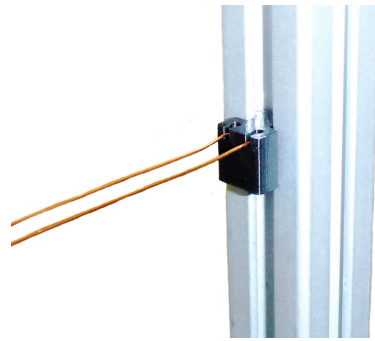


Figure 6.7: Motion restriction bracket.

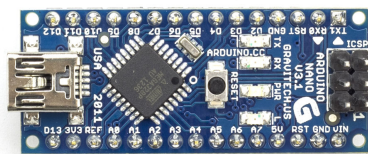
6.4 Pendulum Module

6.4.1 The electronics

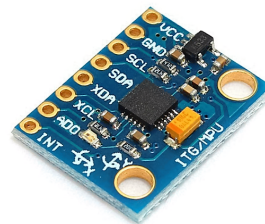
Given the size and purpose requirements I was limited by, it would be beneficial to design a dedicated PCB (Printed Circuit Board) that would accommodate all of the necessary electronic components and ports. However, because of this being a first prototype which should mainly serve as a proof of concept device, fabricating a custom PCB is both too expensive and laborious task. Therefore, I decided to use Arduino¹¹ open-source electronic prototyping platform and compatible third-party components, all in form of breakout-boards, which already accommodate required circuitry and are mostly ready to be wired up.

Main Processing Unit

With spatial limitations on mind, I selected the Arduino Nano 3.0 board as the central processing unit of the module. More details and complete technical specification of this board can be found at [4].



(a) : Arduino Nano 3.0 from [4].



(b) : IMU module GY-521.

Figure 6.8: Pictures of the electronic components.

¹¹<http://www.arduino.cc>

■ Inertial Measurement Unit

There are several inertial measurement sensors available within the Arduino compatible electronic parts. In most cases, these utilize a MEMS¹² three-axis accelerometer and gyroscopic sensor plus, in some cases, a magnetometer. The purpose of the magnetometer in such application is to measure the Earth magnetic field, acting as a compass, in order to refine the measurement of the position about the horizontal axis. However, such sensor' function can be easily spoiled by the presence of a nearby artificial magnetic field which happens to be exactly my case. Therefore, I chose the unit without the magnetometer, namely the MPU 6050 sensor from InvenSense [5], specifically the GY-521 sensor board.

Big advantage of this sensor unit is a small on-chip Digital Motion ProcessorTM (DMP). This DMP can be programmed with firmware and allows to proceed complex calculations with the sensor values directly on the sensor board, providing the orientation data in desired format¹³ on its output, which significantly reduces the computational load on the Arduino microcontroller.

■ Coil Power Supply

Controlling the current through the coil—which is in fact regulating the input voltage—is a similar task to e.g. controlling a DC motor. Therefore, a H-Bridge driver circuit is ideal for such purpose. The estimated current required for generating strong enough magnetic field is about 1 A¹⁴ and the accepted supply voltage should be at least 24 V.¹⁵ My final choice was the L298N Motor Driver Controller Board Module which is primarily designed for controlling a single stepper motor so it features the dual full H-Bridge drive chip (L298N). Therefore, conveniently, it can drive two coils at the same time. According to the datasheet [6], the driver accepts input voltage up to 35 V and supplies the current up to 2 A on both H-Bridges. However, the maximum power draw is limited at 25 W, which effectively prevents running both coils simultaneously at more than 0.5 A.

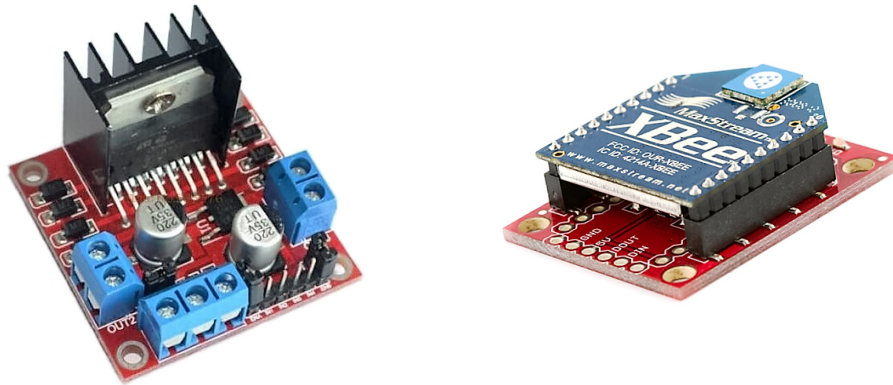
As seen on the Figure 6.9a on the facing page the board is quite sizable compared to the other electronics I used, which is mainly because of the terminal connectors and the bulky thermal diffuser ('heatsink') mounted on the H-bridge chip. Such feature would not be necessary for my application since drawing steady high current for longer time periods is not expected within any kind of experiments on the platform. However, given the shape of the assembly, dismantling the diffuser would save no space and the weight reduction is irrelevant in this case. For the permanent solution, I recommend using a smaller SMD H-Bridge without the thermal diffuser.

¹²Micro-Electro-Mechanical System

¹³E.g. quaternions, Euler angles, etc.

¹⁴This estimation was the result of previous experiments with the first produced coils. Having a thinner wire, these were becoming too hot under current load bigger than 0.8 A. The newest coil design, however, can draw slightly higher current without getting hot too quickly. Fortunately, selected driver is able to supply up to 2 A which is more than enough even for newer coils.

¹⁵Due to the electrical resistance of the coils, lower voltage would not be able to drive sufficiently high current through these.



(a) : L298N H-Bridge module.

(b) : Xbee[®] module.**Figure 6.9:** Pictures of the electronic components.

■ Communication Device

According to the requirements from the Section 5.1 on page 11 and also given by the very principle of multi-agent system, it is essential for the modules to share the information, should that be either measured data or setup and synchronization data. For that purpose, a suitable wireless communication method had to be selected. The application where the devices need to talk and listen to each other prompts using Wi-Fi or Bluetooth standards. However, for the sake of simplicity, size and low cost, I selected ZigBee communication standard, namely the Xbee[®] RF module from the manufacturer Digi¹⁶ with omni-directional on-chip antenna (see the Figure 6.9b). For easier mounting, connecting and programming, I used the SparkFun Xbee Explorer USB module, which features the USB-to-Serial converter for easier connection and communication with PC. It also breaks out the Xbee pins into the pair of headers so it is easy to solder the respective header pins on the ports needed for powering the module and connecting to the Arduino. More information about the product can be found at [7].

ZigBee protocols allow for creating a ‘*mesh*’ type network within a group of compatible devices where individual connections can be defined so the mesh topology exactly matches the module layout. There is a need for single *network coordinator* in the mesh which can either be one of the modules or—and perhaps even more conveniently—an external device which could later serve as a platform controls¹⁷ [8]. ZigBee standard also defines, amongst others, a periodical data transfer which is particularly designed for transferring the data from real-time sensors, just like in my case.

¹⁶<http://www.digi.com/>

¹⁷Allowing to start, stop and maintain the experiments etc.

6.4.2 3D Printed Parts

To assemble all the electronic parts and the coils together into a compact module, I designed several brackets and holders. First bracket **A** shown on the Figure 6.10 is designed to hold both the IMU and the H-Bridge boards. The inertial sensor fits into the rectangular rim '1' in the middle while the two circular pegs '2' help to fasten it in position via the board mounting holes. The strip opening '3' allows for pin headers to be inserted from the bottom side of the sensor board. The H-Bridge module is bolted on top using the holes '4' while longer M3 machine screws are used to secure this section to the rest of the module.

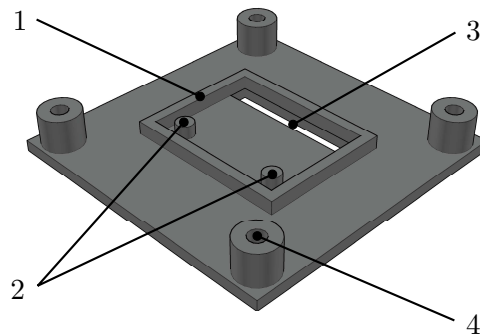


Figure 6.10: Part **A** of the pendulum module.

The biggest part **B** of the module frame seen on the Figure 6.11 accommodates the Arduino Nano 3.0 and partially forms the connection for the coils. The Arduino fits tight into the recessed area '1'. The mounting holes '2' match the mounting holes from the previous part A. The openings '3' and '4' allow for the header pins from the IMU to stick through and to be accessible with wire connectors. The hexagonal holes '5' allows for the standard 20 mm long hex spacers with M3 thread to be inserted. All the other holes and recesses are designed for easier and less tangled wire routing.

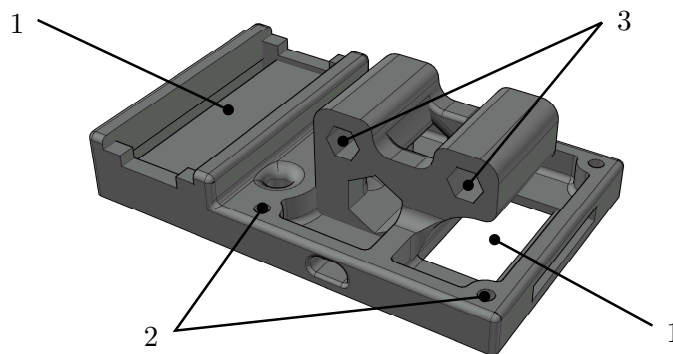


Figure 6.11: Part **B** of the pendulum module.

Last three printed parts form the bracket **C** on the Figure 6.12 on the next page which allows for fastening the XBee module. Once again there are hexagonal holes for the hex spacers while these also hold all three parts of the bracket together. In the middle of the part 'c₁' there is also a vertical hole with hexagonal recess on the

bottom side. That allows for the M5 nut to be pressed into so the whole bracket can be screwed onto the aluminium pendulum rod.

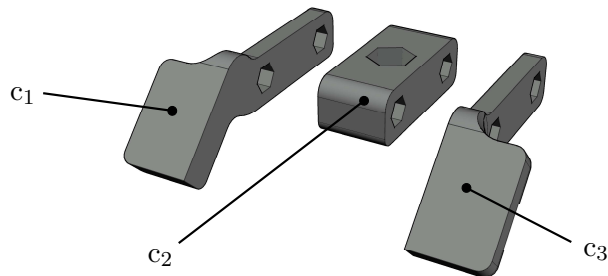
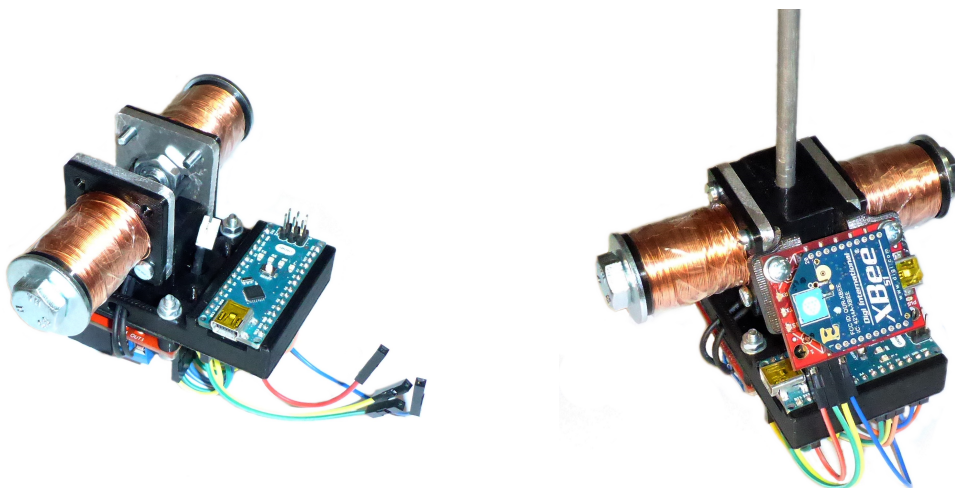


Figure 6.12: Part C of the pendulum module.

6.4.3 Module Assembly

As mentioned in the previous section, segments **A** and **B** are screwed together along with the H-Bridge module. Next, two coil assemblies can be fastened from each side onto the inserted hexagonal spacers. This segment finished and wired up is on the Figure 6.13a. There is a dual conductor cable with white connector sticking out on the top—that is the power and ground cable which can connect to its opposing end which comes out of the pendulum rod. That is to allow for this main part of the module to be separated from the rest of the platform, at the time mainly for easier manipulation and maintenance.



(a) : Main module segment.

(b) : Module fully completed.

Figure 6.13: Pictured of the final module assembly.

The Xbee module mounts, however, onto the top bracket C which is meant to be screwed onto the rod permanently, which is not only because of the tight screw fit but also because of the fact that the power cable connector can not go through the M5

screw hole. That is an undesired result of a late decision upon what communication technology to use. At the time when I chose XBee, the main part of the module was already finalized after several design iterations and I did not manage to find an easy way how to add the XBee module onto the existing assembly without it sticking out too much. With this solution the fully assembled module looks quite compact and the only disadvantage is the need for unscrewing the XBee every time the module is about to be disconnected.¹⁸ After connecting the power cable, main module assembly is fastened to the rod bracket via four M3 machine screws through the remaining screw holes on the coil assemblies into the hex spacers. Lastly, XBee module is connected via jumper wires. The finished module secured to the rod is on the Figure 6.13b on the previous page.

¹⁸The obvious alternative is simply unplugging the wires from XBee module while leaving it fastened to the bracket.



Part II

Mathematical Model

Chapter 7

General Mathematical Model

In this section I derive the mathematical description for 2D array version of the platform while considering the square matrix layout for the pendulums. The model only deals with the dynamics of the mechanical part of the system – the dynamics of the electrical part including the transient response of the coils is typically faster by several orders of magnitude.¹

The equations of the system dynamics are compiled for a single module and the possibility of input force is expected in both x and y direction. The differential equations (DEs) are derived using the Lagrange's approach in the Section 7.2 on the following page. Due to the systems nature however, I used a nonstandard generalized coordinates for describing the spherical pendulum dynamics. The reason for selecting such parametrization is explained in the Section 7.2.1 on the next page, while more throughout discussion about the advantages of certain parametrization with respect to the given device and task is provided in [9]. Although it is not my intention to explain the Lagrange's formalism in detail, each significant step of the derivation along with the corresponding partial result is provided and commented throughout the following sections.

7.1 Simplifying Assumptions

Before I begin compiling the equations I need to make several assumptions regarding the physical system to clearly define the complexity of the model I am trying to accomplish. It is important to decide which physical phenomena are important for the system dynamics and which can be neglected without significant reduction of the model accuracy. The assumptions are following.

- Each component of the system is infinitely stiff. There are no flexible parts,
- Universal joint acting as a spherical hinge is considered ideal, introducing an even damping for all directions,
- Pendulum module can be approximated with its center of mass,
- Pendulum rod is considered massless,

¹This may not apply for the coils with big hysteresis caused by the core made from magnetically hard material.

- Only viscous damping is considered. Any other forms of damping are neglected,
- There are no external disturbance torques applied on the system.

There is one more important fact to acknowledge. The mathematical model I am about to derive does not consider possible collisions of the modules. This is nearly inevitable property of the model because it is extremely complicated to describe the dynamics of the impacts and bounces that happen during the collisions with just a system of DEs. It is a common practice to use hybrid models in order to describe systems with such properties. Hybrid models introduce a discrete variables, so called ‘modes’ and for each mode, there can be different set of DEs. Unfortunately, in my case the collisions are simply too complex. There are infinitely many ways for two neighbours to collide, moreover the resulting motion depends not only on the initial velocities and momentums but also on the magnetic interactions. Ultimately, it is hardly an achievable task to sufficiently describe the collisions in the model. Perceiving this along with the fact that collisions are unwanted during the experiments, I stick with non-collision model and consider a *collision avoidance* as one of the key tasks for the control algorithms possibly developed in the future.

7.2 Lagrange’s Equations

7.2.1 Generalized Coordinates

Typical parametrization for the classical spherical pendulum is shown on the Figure 7.1a on the facing page and uses standard spherical coordinates ϕ and θ . Such coordinates are particularly convenient because of the elementary transformation into the cartesian coordinates

$$\begin{bmatrix} x, y, z \end{bmatrix}^T = \begin{bmatrix} l \cos \phi \sin \theta, l \sin \phi \sin \theta, l \cos \theta \end{bmatrix}^T, \quad (7.1)$$

which guarantees simple equations for both potential and kinetic energy and consequently quite simple Lagrange’s equations.

My choice of the vector of generalized coordinates $\mathbf{q} = [\varphi, \psi]$ indicated on the Figure 7.1b on the next page does not have this convenient property while its transformation is much more complicated. It has, however, a property of $\pi/4$ rotational symmetry along the z -axis which mimics the real system. Furthermore, within the expected range of motion, my selected coordinates correspond almost perfectly to the angles measured by the IMU described in the Section 6.4.1 on page 22, and also to the angles in the universal joint double hinge mechanism. Therefore, if there is any disproportion in the damping,^{2,3} I can easily adjust it by just changing the value of damping for either φ or ψ equation. Last advantage of this parametrization is that both coordinates are ‘equal’ with respect to the system geometry. Such property causes that all the equations for these coordinates will look exactly the same with only the coordinates swapped.

²E.g. one part of the joint is stiffer than the other.

³In the Section 7.1 on the previous page I first assumed the damping to be even. However, given by the universal joint mechanism, I may need to withdraw this assumption.

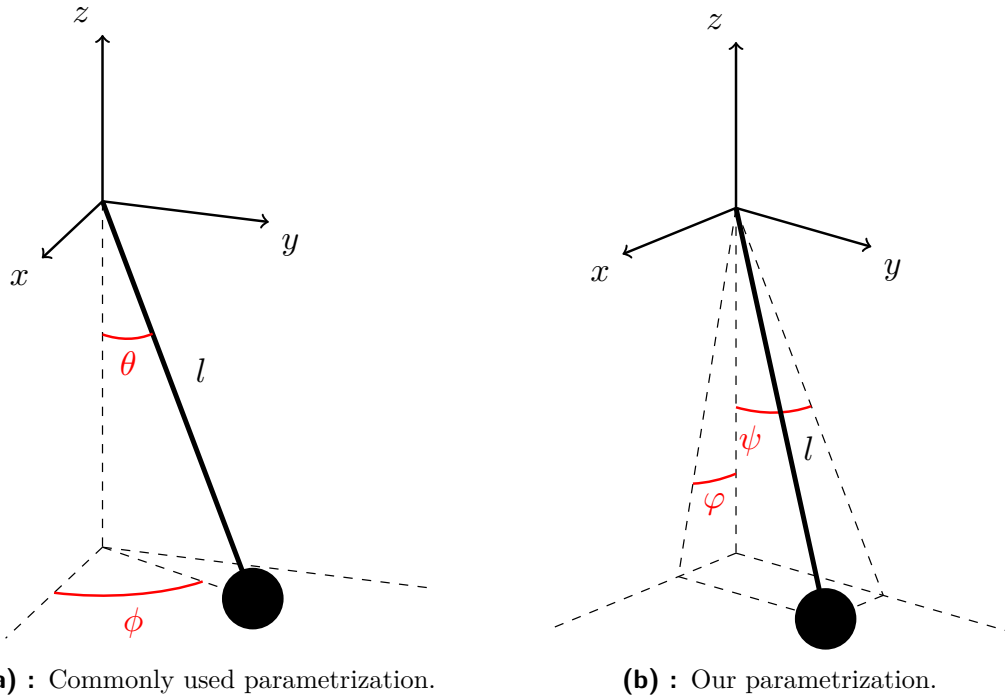


Figure 7.1: Two alternative selections of generalized coordinates for the spherical pendulum system.

According to the trigonometry formulas for φ and ψ and 3D analogy of the Pythagorean theorem, for cartesian coordinates x , y , and z we can write

$$\tan \varphi = \frac{x}{-z} \tag{7.2}$$

$$\tan \psi = \frac{y}{-z} \tag{7.3}$$

$$l^2 = x^2 + y^2 + z^2. \tag{7.4}$$

Substituting for the x and y in the Equation (7.4) from the Equations 7.2 and 7.3 respectively, we get

$$l^2 = z^2 \tan^2 \varphi + z^2 \tan^2 \psi + z^2, \tag{7.5}$$

which can be solved for z as

$$z = \sqrt{\frac{l^2}{\tan^2 \varphi + \tan^2 \psi + 1}}. \tag{7.6}$$

Now let's apply several equivalent operation to the expression under the square root

$$\begin{aligned}
\frac{l^2}{\tan^2 \varphi + \tan^2 \psi + 1} &= \frac{l^2}{\frac{\sin^2 \varphi}{\cos^2 \varphi} + \frac{\sin^2 \psi}{\cos^2 \psi} + 1} \\
&= \frac{l^2}{\frac{\sin^2 \varphi \cos^2 \psi + \sin^2 \psi \cos^2 \varphi + \cos^2 \varphi \cos^2 \psi}{\cos^2 \varphi \cos^2 \psi}} \\
&= \frac{l^2 \cos^2 \varphi \cos^2 \psi}{\sin^2 \varphi \cos^2 \psi + \sin^2 \psi \cos^2 \varphi + \cos^2 \varphi \cos^2 \psi} \\
&= \frac{l^2 \cos^2 \varphi \cos^2 \psi}{\sin^2 \varphi \cos^2 \psi + \cos^2 \varphi (\sin^2 \psi + \cos^2 \psi)} \\
&= \frac{l^2 \cos^2 \varphi \cos^2 \psi}{\sin^2 \varphi \cos^2 \psi + \cos^2 \varphi}.
\end{aligned}$$

By substituting back to the Equation (7.6) on the previous page and simplifying the term we get

$$z = \frac{l \cos \varphi \cos \psi}{\sqrt{\sin^2 \varphi \cos^2 \psi + \cos^2 \varphi}}, \quad (7.7)$$

and combining the Equation (7.7) with the Equations 7.2 and 7.3, x and y can be expressed as

$$x = \frac{l \sin \varphi \cos \psi}{\sqrt{\sin^2 \varphi \cos^2 \psi + \cos^2 \varphi}} \quad (7.8)$$

$$y = \frac{l \cos \varphi \sin \psi}{\sqrt{\sin^2 \varphi \cos^2 \psi + \cos^2 \varphi}}. \quad (7.9)$$

The Equations 7.8, 7.9 and 7.7 define the sought transformation. Obviously, the common square root term in the denominator is unfortunate as it makes all the further derivations, especially the derivatives, much more complex. However, by examining the properties of this function

$$f(\varphi, \psi) = \sqrt{\sin^2 \varphi \cos^2 \psi + \cos^2 \varphi}, \quad (7.10)$$

we find out that it is equal to 1 for zero angles and for small angles $\varphi < 10^\circ$ and $\psi < 10^\circ$, this term remains very close to 1 - the maximum deviation from 1 is $\epsilon < 0.0005$. Since the estimation for maximal actual angles is about 5° , we can completely neglect this term, ending up with much simpler transformation

$$[x, y, z]^T = [l \sin \varphi \cos \psi, l \cos \varphi \sin \psi, l \cos \varphi \cos \psi]^T. \quad (7.11)$$

7.2.2 Energies in the System

In Lagrange's approach to modeling it is essential to evaluate the total potential energy \mathcal{V} and kinetic energy \mathcal{T} in the system. Since I consider the pendulum to be single rigid body approximated by its center of mass, both energies only have one member. Evaluating the potential energy is straightforward.

$$\mathcal{V} = -m g z = -m g l \cos \varphi \cos \psi, \quad (7.12)$$

where m [kg] is the mass of the pendulum and $g = 9.81 \text{ m s}^{-2}$ is the Earth's gravitational acceleration.

For the kinetic energy

$$\mathcal{V} = \frac{1}{2} m \mathbf{v}^2, \quad (7.13)$$

we need to evaluate the square of the velocity

$$\mathbf{v}^2 = \dot{x}^2 + \dot{y}^2 + \dot{z}^2. \quad (7.14)$$

Due to my parametrization unfortunately, the sum of these squares of derivatives can not be simplified into as convenient expression as the other parametrization on the Figure 7.1a on page 31 provides. The expression, however, can be written as

$$\mathbf{v}^2 = l^2 \left[\dot{\varphi}^2 + \dot{\psi}^2 - \left(\dot{\varphi} \cos \varphi \sin \psi - \dot{\psi} \sin \varphi \cos \psi \right)^2 \right], \quad (7.15)$$

and we can once again use the fact of limited range of motion to simplify this expression. Using the approximation

$$\text{if } \alpha \approx 0 \text{ then } \sin \alpha \approx \alpha \text{ and } \cos \alpha \approx 1, \quad (7.16)$$

we can rewrite the Equation (7.15) as

$$\mathbf{v}^2 = l^2 \left[\dot{\varphi}^2 + \dot{\psi}^2 - \left(\dot{\varphi} \psi - \dot{\psi} \varphi \right)^2 \right]. \quad (7.17)$$

Now for small φ and ψ we can write that

$$\dot{\varphi}^2 + \dot{\psi}^2 \gg \left(\dot{\varphi} \psi - \dot{\psi} \varphi \right)^2 \text{ for } \dot{\varphi} \neq 0 \text{ or } \dot{\psi} \neq 0, \quad (7.18)$$

and neglect the term in brackets consequently, obtaining a simple equation for the square of the velocity⁴

$$\mathbf{v}^2 = l^2 \left(\dot{\varphi}^2 + \dot{\psi}^2 \right). \quad (7.19)$$

Even though it may seem that I just committed some major simplification, the actual impact on the model precision is very minimal, especially compared to the effect of the simplifying assumptions I made in the Section 7.1 on page 29 or to other errors that are likely to be introduced by inaccurate measurements of physical parameters.

Finally, the completed Lagrangian can be written as

$$\mathcal{L}(\mathbf{q}, \dot{\mathbf{q}}) = \mathcal{T} - \mathcal{V} \quad (7.20)$$

⁴We must not forget that this is only the approximation valid for small angles φ and ψ .

7.2.3 Differential Equations

The general expression for the Lagrange's equations is

$$\frac{d}{dt} \frac{\partial \mathcal{L}(q, \dot{q})}{\partial \dot{q}_i} - \frac{\partial \mathcal{L}(q, \dot{q})}{\partial q_i} + \frac{\partial \mathcal{D}(\dot{q})}{\partial \dot{q}_i} = Q_i, i = 1, 2, \quad (7.21)$$

where q_i and \dot{q}_i are the i -th elements of the vector of generalized coordinates $\mathbf{q} = [\varphi, \psi]$ and vector of generalized velocities $\dot{\mathbf{q}} = [\dot{\varphi}, \dot{\psi}]$ respectively, Q_i is the i -th element of the vector of generalized input torques⁵ and $\mathcal{D}(\dot{q})$ is a dissipative function. Everything but the last two members is already available from previous derivations so let us closer inspect the remaining.

Dissipative function comprises all mechanic energy losses in the system.⁶ According to the assumptions stated in section Section 7.1 on page 29, the only losses are caused by the viscous damping in the pendulum spherical hinge. Since the universal joint used for that hinge is basically just two simple hinges with perpendicular axes and the angle in these hinges correspond to generalized coordinates φ and ψ ⁷, we can write the expression for the dissipative function

$$\mathcal{D}(\dot{\varphi}, \dot{\psi}) = \frac{1}{2} b_\varphi \dot{\varphi}^2 + \frac{1}{2} b_\psi \dot{\psi}^2. \quad (7.22)$$

Finally there is a vector of generalized torques which comprises all torques and forces affecting the system. Respecting the assumptions once again, the only input to the system are the magnetic forces F_i , $i = 1, 2, 3, 4$ in four possible interactions between the inspected module and its four neighbours. As I already mentioned in the Section 5.1 on page 11, the mutual force interaction depends on the electric currents through both opposing coils and the position of both modules within the horizontal plane. Therefore, for each of these forces, we can write

$$\mathbf{F}_i = \mathbf{F}_i(x_0, y_0, x_i, y_i, i_0, i_i), \quad (7.23)$$

where $[\mathbf{x}_0, \mathbf{y}_0]$ and $[\mathbf{x}_i, \mathbf{y}_i]$ are the cartesian coordinates of inspected module and its i -th neighbour and i_0 and i_i are the the respective currents. Of course, the value also depends on multiple fixed parameters, some of which I know (e.g. the number of turns in coils N , magnetic permeability of the air μ) but many of which are unknown and very difficult to measure—the shape of the magnetic fields or the magnetic permeability of the coil cores to name a few (more throughout discussion on this topic can be found in [10]). Furthermore, there are many formulas for the magnetic flux density describing some idealized elementary instances⁸ but no universal formula that would accept all of these arguments and provided reliable results.

Ultimately, finding a sufficiently accurate algebraic expression for \mathbf{F}_i using just an analytic methods is extremely difficult. Using some methods of identification

⁵In general terminology, a generalized torque stands for both torque and force because the vector may contain either, depending on the generalized coordinates. In my case, the coordinates have angular dimension, thus I am considering torques.

⁶These losses are mostly in form of irreversible conversion of the mechanical energy to the heat energy.

⁷For small φ and ψ .

⁸Such as point source of the field, infinitely big magnetic surface etc.

followed by interpolation of the results is more likely to be successful. This issue is further discussed in the Chapter 8 on page 39.

Even though we do not know the exact formula for the force inputs, we can still proceed to finishing Lagrange's equations. However, we need to know how to translate these forces into torques τ_φ and τ_ψ which we need in the equations. Let's first take a top view onto the situation where module \mathbf{M}_0 attracts with its neighbour \mathbf{M}_i as illustrated on the Figure 7.2.

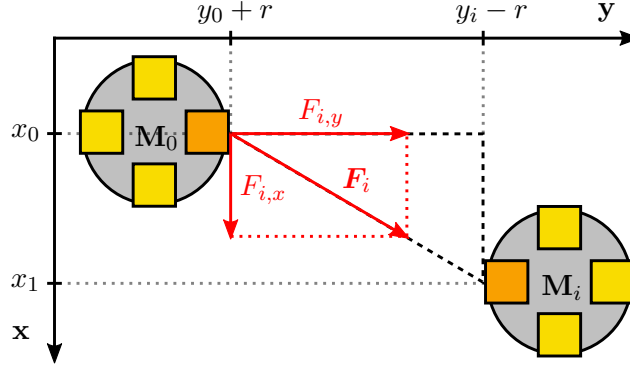


Figure 7.2: Decomposition of the force acting on the module \mathbf{M}_0 viewed from above. The orange squares represent the coils, darker coils are active in the interaction.

As long as we assume that both attractive and repulsive forces act along the line that connects the ends of the opposing coils and such point is in the distance r from the center of the module, we can decompose such force \mathbf{F}_i into its x and y components $F_{i,x}$ and $F_{i,y}$. With the use of the similar triangles we can write for the components

$$F_{i,x} = \mathbf{F}_i \cos \alpha \quad \text{and} \quad F_{i,y} = \mathbf{F}_i \sin \alpha \quad \text{where} \quad \alpha = \arctan \frac{x_i - x_0 - 2r}{y_i - y_0 - 2r}, \quad (7.24)$$

and the respective torques are

$$\tau_{\varphi,i} = F_{i,x} l \quad \text{and} \quad \tau_{\psi,i} = F_{i,y} l, \quad (7.25)$$

where l is the length of the pendulum rod. We apply this method on all four neighbours and the sought total torques are

$$\tau_\varphi = \sum_{i=1}^4 \tau_{\varphi,i} \quad \text{and} \quad \tau_\psi = \sum_{i=1}^4 \tau_{\psi,i}. \quad (7.26)$$

Finally, we can evaluate the Equation (7.21) on the facing page and get the complete set of two nonlinear 2nd differential equations (DEs)

$$m l^2 \ddot{\varphi} - m g l \dot{\varphi} \sin \varphi \cos \psi + b_\varphi \dot{\varphi} = \tau_\varphi \quad (7.27)$$

$$m l^2 \ddot{\psi} - m g l \dot{\psi} \sin \psi \cos \varphi + b_\psi \dot{\psi} = \tau_\psi. \quad (7.28)$$

Reusing the approximation for small φ and ψ we can further simplify these into its final form

$$m l^2 \ddot{\varphi} + b_\varphi \dot{\varphi} - m g l \dot{\varphi} \varphi = \tau_\varphi \quad (7.29a)$$

$$m l^2 \ddot{\psi} + b_\psi \dot{\psi} - m g l \dot{\psi} \psi = \tau_\psi. \quad (7.29b)$$

7.3 State Space Model

For numeric simulations, I wanted to implement the derived mathematical model in MATLAB[®]. As powerful as it is, however, this software can not handle a system with higher order DEs directly. For simple equations, there is an option to ‘wire up’ the block diagram manually in Simulink^{®9} but for more complicated equations, this would be rather tedious task. It is much more convenient to substitute each n -th order DE with a set of n 1st order differential equations. Resulting set of equations is usually referred to as a *state space* model. Such description can then be easily implemented in MATLAB as a single function.

First let’s introduce a state vector $\mathbf{x}(t)$ and input vector $\mathbf{u}(t)$ as

$$\mathbf{x}(t) = [\dot{\varphi}, \dot{\psi}, \varphi, \psi]^T \quad (7.30)$$

$$\mathbf{u}(t) = [\tau_\varphi, \tau_\psi]^T. \quad (7.31)$$

Next step is rewriting the 2nd order DEs 7.29a and 7.29b into following form

$$\ddot{\varphi} = -\frac{b_\varphi}{m l^2} \dot{\varphi} + \frac{g}{l} \dot{\varphi} \varphi + \frac{1}{m l^2} \tau_\varphi \quad (7.32)$$

$$\ddot{\psi} = -\frac{b_\psi}{m l^2} \dot{\psi} + \frac{g}{l} \dot{\psi} \psi + \frac{1}{m l^2} \tau_\psi, \quad (7.33)$$

which only involves basic equivalent operations with the system of equations. The equations (7.32) already make for two of the state equations. For better clarity within selected notation, let’s just relabel them using $\mathbf{x}(t)$ and $\mathbf{u}(t)$.

$$\dot{x}_1 = -\frac{b_\varphi}{m l^2} x_1 + \frac{g}{l} x_1 x_3 + \frac{1}{m l^2} \tau_\varphi \quad (7.34)$$

$$\dot{x}_2 = -\frac{b_\psi}{m l^2} x_2 + \frac{g}{l} x_2 x_4 + \frac{1}{m l^2} \tau_\psi. \quad (7.35)$$

Second two state equations are simply

$$\dot{x}_3(t) = x_1 \quad (7.36)$$

$$\dot{x}_4(t) = x_2. \quad (7.37)$$

Along with the Equations 7.24, 7.25 and 7.26 for deriving τ_φ and τ_ψ , the theoretical function for the force in the Equation (8.3) on page 40 and the transformation function in the Equation (7.11) on page 32, this state space model provides a complete description of a single pendulum and can be treated as a sub-system within the full

⁹A block diagram environment integrated with MATLAB.

system of the platform. In order to do that properly, let's define the inputs and outputs of such subsystem.

$$\text{IN} = [\mathbf{i}, \mathbf{N}_1, \mathbf{N}_2, \mathbf{N}_3, \mathbf{N}_4] \quad (7.38)$$

$$\text{OUT} = [\mathbf{O}_1, \mathbf{O}_2, \mathbf{O}_3, \mathbf{O}_4], \quad (7.39)$$

where

$$\mathbf{i} = [i_1, i_2, i_3, i_4] \quad (7.40)$$

is the vector of control input currents,

$$\mathbf{N}_i = [x_{N,i}, y_{N,i}, i_{N,i}] \quad (7.41)$$

is the output of the i -th neighbour, consisting of the electric current i_{N_i} on its respective coils and the position coordinates x_{N_i} , y_{N_i} in the cartesian frame of the horizontal plane, and

$$\mathbf{O}_i = [x, y, i_i] \quad (7.42)$$

is the output vector of the described module for the i -th neighbour, carrying the same respective information.

The last thing that needs to be defined in each such sub-system is the initial position vector \mathbf{r}_{init} of the represented pendulum within the horizontal coordinate frame of the platform. Accordingly implemented sub-system in Simulink is provided in `.slx` format on the enclosed CD and such blocks can be easily connected together in order to create desired platform layout. One thing that needs to be remembered is that as this model can not deal with collisions, the distance of the adjacent modules must always be greater than zero.

Chapter 8

System Parameters and Identification

In this chapter, I briefly address the problem of measuring or identifying the system parameters for the pendulum platform. These are needed for completion and successful numeric simulation of the mathematical model in MATLAB need to be reasonably accurate for the model to be usable for control algorithms design. Retrieving fixed system parameters important for pendulum dynamics is described in the following Section 8.1, the Section 8.2 on the following page deals with possible methods of identification of the force effects of the magnetic field.

Described methods and procedures are proposals for the further work. The actual measurements and identification were not executed within this thesis, mainly because of the late completion of the prototype. However, it would be useful to test the methods proposed in the Section 8.2.1 on page 41, which the prototype is feasible for.

8.1 Pendulum Characteristics

For my simplified pendulum model, the characteristics is determined by four static parameters. Two of these, the mass m [kg] and the length of the pendulum rod l [m] can be easily measured. The remaining parameters are the viscous damping coefficients b_φ , b_ψ [N ms/rad] in the dual hinge joint. To identify one of these, let's say the b_φ , we first need to restrict the pendulum motion¹ so the angle ψ can not change. Then we need to measure the waveform pendulum deflection φ response to the initial velocity.² According to the assumption that in this setup, our pendulum performs as a dampened mechanical harmonic oscillator, we can use the waveform to determine the logarithmic decrement δ as

$$\delta = \frac{1}{n} \ln \frac{A_1}{A_n} = \frac{b_\varphi n T}{2I}, \quad (8.1)$$

where A_1 and A_n are the first and the n -th amplitude, T is the period of the oscillations and $I = ml$ is the moment of inertia of the pendulum with respect to the hinging axis. Then for b_φ we can write

$$b_\varphi = \frac{2\delta ml}{nT}. \quad (8.2)$$

¹Possible method for this restriction was proposed in the Section 6.3 on page 19.

²Simply pop the pendulum by hand so it starts swinging.

For b_ψ the procedure is almost identical, it only involves locking the motion in φ instead of ψ .

The data of the waveform itself can be measured either with absolute position measuring device in the pendulum module (see the Section 5.3 on page 14), or, in case of its unavailability or insufficient accuracy, using a stationary camera setup and a detecting a distinct point³ on the pendulum module.

8.2 Force Interaction

Finding a reliable mathematical description for the magnetic force between the modules remains the greatest challenge of the whole modeling task. Let's recall and expand what I already stated in the Section 7.2.3 on page 34. The variables that influence the magnitude and the sense⁴ of the mutual force interaction are the positions of the modules and the electric currents through both coils. According to my previous assumptions, I only consider the position within the horizontal plane, changing of the vertical coordinate z is neglected. That allows me to only inspect the relative position of the interacting modules instead of the absolute positions of each. Then the function for the force \mathbf{F} between the modules M_0 and M_1 can be written as

$$\mathbf{F} = \mathbf{F}(\Delta x, \Delta y, i_0, i_1), \quad (8.3)$$

where $\Delta x = x_1 - x_0$ and $\Delta y = y_1 - y_0$ are the relative coordinates and i_0 and i_1 are the electric currents. Now it would be tempting to further simplify this by using the distance d

$$d = \sqrt{\Delta x^2 + \Delta y^2} \quad (8.4)$$

in order to reduce the number of independent arguments down to three. Sadly, we can not do that. The magnetic field around the coils is not the same in all directions in the horizontal plane and therefore it depends on both the distance and the relative orientation of the coils. Furthermore, depending on the geometry of given orientation, not only attractive or repulsive forces but also a torque may act on the coils. And although the setup I propose on the prototype back in the Section 6.3 on page 19 does not allow the modules to rotate, the very presence of such torques influence the resulting force \mathbf{F} . Therefore we need to stick with the function in the Equation (8.3).

Now let's assume that it is possible to rewrite such function as a product of generally nonlinear partial functions

$$\mathbf{F} = f_\Delta(\Delta x, \Delta y) f_i(i_0, i_1). \quad (8.5)$$

This is only a hypothesis, yet it complies with the general form of most known formulas regarding the magnetic force, which can be written as

$$\mathbf{F}_{\text{mag}} = \frac{f_1(B)}{f_2(\text{dist})}, \quad (8.6)$$

³E.g. red dot stucked onto the module.

⁴Attraction or repulsion.

where $B \propto i$ is the magnetic flux density and $dist$ is the distance. Such expression is easily convertible to the form in the Equation (8.5) on the preceding page. This distribution allows me to examine functions f_r and f_i separately, which is much easier than dealing with the original function \mathbf{F} with four arguments.

8.2.1 Force Measurement

The suggested procedure of identification is similar for both functions and is based on manual measurement using a digital force gauge. The key is to measure the force for sufficiently many points from the specified domain of definition of given functions so the data can be then numerically interpolated. For the f_i the domain is given by electric current limitations, generally it is

$$D(f_i) \in \langle -i_{\max}, i_{\max} \rangle \times \langle -i_{\max}, i_{\max} \rangle [A], \quad (8.7)$$

yet, thanks to the expected symmetry of the function f_i^5 , the most efficient way is to select the set M of discrete values from the interval $\langle -i_{\max}, i_{\max} \rangle$ and then to measure the force for all combinations⁶ of $i_0 \in M$ and $i_1 \in M$.

The domain of the position function f_Δ is limited by the range of motion of the modules but we can expect the force to be nearly zero for greater distances. Therefore it is useful to experimentally find the threshold values for $\Delta_{x,\max}$ and $\Delta_{y,\max}$ beyond which the force is negligible. Note that thanks to the axial symmetry of the magnetic field about the coil rotational axis, it is sufficient to do the measurements on only one side of this axis (see the Figure 8.1).

During the measurements for the function f_i it is critical for the modules to be at the same relative position for all measurements. Therefore it is recommended to do this measurement with one module completely fixed and the other restricted in single plane so it is easier to maintain the position.

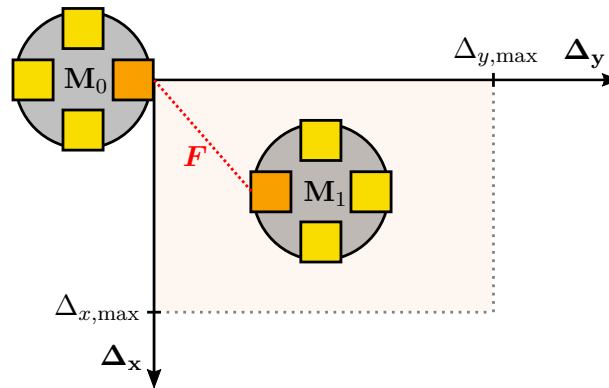


Figure 8.1: Area for measuring the force-position characteristics viewed from above.

For the f_Δ measurements one fixed module remains but this time the other module has to be able to move. The recommended method for executing the measurement is to combine and synchronize the data from the digital force gauge and the position

⁵ $f_i(a, b) = f_i(b, a)$

⁶The order is irrelevant

sensor. That way it is possible to achieve nearly continuous measurements along the lines by pushing or pulling the free module with the force gauge from smaller towards greater distance from the fixed one. Similar approach to the magnetic force, although in simpler form, measurement is described in [11].



Chapter 9

Conclusion

The major objectives of this thesis were to design and build the experimental platform for visualizing and experimenting with wave phenomena in multi-agent system. The platform should have consisted of an array of individually programmable modules capable of mutual force interaction. Due to the reasons which I described in the Section 1.2 on page 1 and further elucidated in the chapters of the Part I, the platform has not been finished in its full desired form. Instead, I designed and built a proof-of-concept prototype of such platform, upon which I tested the core principles and the physical implementations involving mechanical and electrical part, which can now be utilized for extending the platform to its complete shape.

In Chapters 2, 3 and 4, I determined the basic nature of the platform—each module hangs on a rigid rod, forming a spherical pendulum, and uses electromagnets to interact with the adjacent modules.

In the Chapter 5, I described what features regarding measurement are necessary for the proper function of the platform. After that, in the the Chapter 6, I dealt with the actual implementation of selected concept. Namely I determined the size of the modules according to the estimated sized of its components and the size of the whole platform consequently, handled the physical properties and fabrication of the actuating coils, designed and produced the parts for the module frame in order to accommodate the coils and all the required electronic parts and ultimately assembled two of the prototype pendulum modules.

In the Part II, I describe the derivation of the mathematical model for one module within the platform in its full desired form. The model describes the dynamics of the mechanical part, thus the dynamic motion of the module including the interaction with possible neighbours. As such, it can be easily extended for whole platform, regardless of the number of modules or the topology, as long as it remains a regular 1D or 2D array. I used Lagrange's equations to extract the differential equations, which I then transferred onto a state space model, which I also implemented in Matlab. The greatest weakness of the model is the fact that it does not consider the collisions of the modules. Therefore, for the proper function of the model, collisions have to be avoided, ideally with the use of some collision avoidance control algorithm.

Lastly, in the Chapter 8, I suggest the methods of system identification that provide the concrete values for the parameters in the mathematical model and also a method of measuring the force interaction between the modules to obtain a set of data which can be further interpolated in order to get the approximated function for the magnetic force.



Bibliography

- [1] *GP2Y0A51SK0F Distance Measuring Sensor Unit*. [datasheet] ©2016 Sharp Corporation, Online: http://www.sharp-world.com/products/device/lineup/data/pdf/datasheet/gp2y0a51sk_e.pdf (Cited on 21 May, 2016)
- [2] *VL6180X Proximity and Ambient Light Sensing Module*. [datasheet] STMicroelectronics, Online: <http://www.st.com/content/ccc/resource/technical/document/datasheet/c4/11/28/86/e6/26/44/b3/DM00112632.pdf/files/DM00112632.pdf/jcr:content/translations/en.DM00112632.pdf> (Cited on 21 May, 2016)
- [3] K. Halbach. *Design of permanent multipole magnets with oriented rare earth cobalt material*. Nuclear Instruments and Methods, Volume 169, Issue 1, p. 1-10, 1980. Online: <http://www.askmar.com/Magnets/Permanent%20Multipole%20Magnets%20Design.pdf> (Cited on 13 April, 2016)
- [4] *Arduino Nano product page*. ©2016 Arduino, Online: <https://www.arduino.cc/en/Main/ArduinoBoardNano> (Cited on 21 May, 2016)
- [5] *MPU-6000 and MPU-6050 Product Specification, Revision 3.4, 18 September, 2013*. [datasheet] InvenSense Inc., Online: https://store.invensense.com/datasheets/invensense/MPU-6050_DataSheet_V3%204.pdf (Cited on 21 May, 2016)
- [6] *Dual Full-Bridge Driver, January, 2000*. [datasheet] STMicroelectronics, Online: <http://www.st.com/content/ccc/resource/technical/document/datasheet/82/cc/3f/39/0a/29/4d/f0/CD00000240.pdf/files/CD00000240.pdf/jcr:content/translations/en.CD00000240.pdf> (Cited on 21 May, 2016)
- [7] *SparkFun XBee Explorer USB product page*. SparkFun Electronics®, Online: <https://www.sparkfun.com/products/11812> (Cited on 21 May, 2016)
- [8] *XBee and XBee-PRO ZigBee, 2015*. [datasheet] Digi International Inc., Online: http://www.digi.com/pdf/ds_xbee_zigbee.pdf (Cited on 21 May, 2016)
- [9] M. Spong, S. Hutchinson, and M. Vidyasagar. *Robot Modeling and Control*. John Wiley and Sons, New York, 2006.

- [10] M. Zahn. *RES.6-002 Electromagnetic Field Theory: A Problem Solving Approach, Spring 2008*. (Massachusetts Institute of Technology: MIT OpenCourseWare), <http://ocw.mit.edu> (Cited on 22 April, 2016). License: **Creative Commons BY-NC-SA**

- [11] J. Zemánek and Z. Hurák. *Experimental modular platform for distributed planar manipulation by shaping magnetic field*. Submitted for publication. 2015.



Appendices



Appendix A

Contents of the enclosed CD

Directory	Files
123D	Editable 3D designs in Autodesk 123D Design format .123dx.
Printable	3D models exported in .stl format standard for 3D print.
Matlab	Implementation of the State Space model in .slx Format.
Thesis	Text of this thesis in .pdf format.